

Interfacial Properties of Colloidal Model Systems

**Richard Vink, Andres de Virgiliis, Stefan Wolfsheimer, Tanja Schilling,
Jürgen Horbach, and Kurt Binder**

Institut für Physik, Johannes Gutenberg–Universität Mainz
Staudinger Weg 7, 55099 Mainz, Germany
E-mail: {schillit, horbach, kurt.binder}@uni-mainz.de

Monte Carlo (MC) simulations are presented in which the phase behavior of colloid-polymer mixtures and of colloidal liquid crystals is investigated. The simulations demonstrate that colloidal systems are good model systems to study the critical behavior of confined systems and the phase behavior of liquid crystals.

1 Introduction

Colloidal systems consist of big molecules (colloids) with a typical size ranging from about 1 nm to several μm , that are suspended in an atomistic solvent. With respect to the phase behavior, colloids are often similar to atomistic systems. However, in the case of colloids, one can often extract much more detailed information than in comparable atomistic systems. For instance, confocal microscopy can be used to make colloids visible and to measure their trajectories as in a computer simulation. Moreover, in experiment, the effective interactions between the colloids can be tuned to some extent by changing the properties of the solvent. Thus, colloids can be used as model systems for the more complicated atomistic world.

Information that is complementary to that extracted from experiments can be obtained in computer simulations of colloidal systems. From a simulation, thermodynamic quantities such as the free energy of the system can be determined, that are not accessible in an experiment. In addition the simple effective interactions between colloidal particles that can be realized in an experiment are well suited for computer simulations. In this work, we demonstrate this for two examples where “hard core” interactions between colloidal particles are considered. The first part of what follows is devoted to the phase behavior of colloid-polymer mixtures in confinement and the second part is on the phase behavior of colloidal liquid crystals (modeled by hard rods or platelets).

2 Phase Behavior of the Asakura-Oosawa (AO) Model in Confinement

Mixtures of colloids with non-adsorbing polymers are of particular interest because they may exhibit a fluid-fluid phase separation which is of purely entropic origin. This transition is driven by a depletion effect¹: Each colloidal particle is surrounded by a depletion zone from which polymers are excluded. When two colloids are close together, their depletion zones overlap, thereby increasing their free volume, and hence the entropy of the system. If the gain in entropy is sufficient, the system demixes into a colloid-rich phase, the liquid phase, and a colloid-poor phase, the vapor phase. It is of particular interest to consider

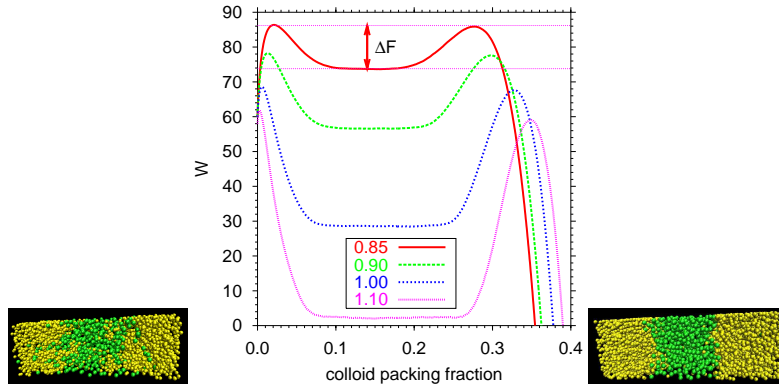


Figure 1. Logarithm of the probability $P(\eta_c)$ of observing a colloidal packing fraction η_c for an AO mixture with $q = 0.8$ at coexistence for several values of η_p^r as indicated. The simulations were performed in a box with $L_x = L_y = 16.7$ and $L_z = 33.4$ using periodic boundary conditions. The snapshots show the system in the phase separated region at $\eta_c = 0.13$ for $\eta_p^r = 0.85$ (left snapshot) and $\eta_p^r = 1.1$ (right snapshot). Polymers and colloids are shown as yellow and green spheres, respectively. From Ref.⁶.

colloid-polymer mixtures confined between walls. In confined geometry, new phenomena are found such as capillary condensation, wetting transitions etc. and near the critical point a crossover scaling from 3D Ising to 2D critical Ising behavior is expected.

As a very simple model for a colloid-polymer mixture we use the so-called Asakura-Oosawa (AO) mixture¹. Here, colloids and polymers are considered as spheres with respective radii R_c and R_p . Hard sphere interactions are assumed between colloid-colloid and colloid-polymer pairs, whereas polymer-polymer pairs can interpenetrate freely. Apart from a bulk system, we also consider a thin film geometry where the system is confined between two parallel hard walls.

In order to study the phase behavior of the AO model, we used Monte Carlo (MC) simulations in the grand canonical ensemble, in which the volume V , the respective fugacities $\{z_c, z_p\}$ of colloids and polymers, and the temperature T are fixed². Note that the number of particles inside V is a fluctuating quantity in the grand canonical ensemble: in a grand canonical move, particles are inserted into the system or removed from it. Since in the AO model all allowed configurations have zero potential energy, temperature plays a trivial role and the phase behavior is controlled by the colloid-to-polymer size ratio q and the fugacities $\{z_c, z_p\}$. We consider here a size ratio $q = 0.8$ and put $R_c \equiv 1$ to set the length scale. One defines the quantity $\eta_p^r \equiv z_p(4\pi/3)R_p^3$, the so-called polymer reservoir packing fraction, which plays a role similar to the inverse temperature in simple fluids. In the bulk case, the simulations are performed in a box with edges $L_x \times L_y \times L_z$ using periodic boundary conditions. In the thin film case, periodic boundary conditions are only applied in the x and y directions, while in the z direction two parallel walls are placed, one at $z = 0$ and the other one at $z = L_z = D$ (with D being the film thickness).

The use of the grand canonical ensemble allows to fully characterize the fluid-fluid demixing transition of the AO model. As we shall see below, finite-size scaling can be applied to determine critical properties, the interfacial tension and other properties of the interface separating the colloid vapor from the colloid liquid phase. However, a common

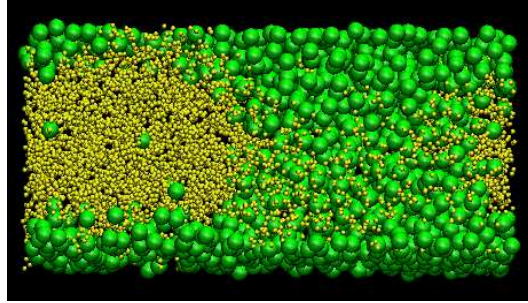


Figure 2. Snapshot of the AO model confined between hard walls ($L_x = L_y = 20$ and $D = 10$) in the phase separated region for $\eta_p^* = 1.1$ and $\eta_c = 0.15$. Polymers and colloids are shown as yellow and green spheres, respectively. Note that the size of the polymers is not at scale to allow for a better visibility of the colloids.

problem of grand canonical MC is a low probability for particle insertions at high densities. In our case, high densities have to be considered due to the presence of the polymers. We have solved this problem by using a cluster move: instead of inserting or removing particles one at a time, clusters of polymers are removed for each colloid that is inserted. The details of this move can be found elsewhere³. Moreover, a reweighting scheme enables the simulation to cross the free energy barrier separating the colloid vapor phase from the colloid liquid phase, and sample the phase-separated regime. Here, we use successive umbrella sampling the details of which can be found in the original reference⁴.

The grand canonical MC yields the probability $P(\eta_c)$ that a certain colloid packing fraction $\eta_c = (4\pi/3)R_c^3 N_c/V$ is observed, i.e. one obtains a histogram counting how often a certain colloid packing fraction has occurred. If phase separation emerges, the distribution $P(\eta_c)$ is bimodal. Fig. 1 shows the logarithm of distributions for different values of η_p^* . Note that $-\ln(P)$ is proportional to the free energy of the system. The peaks at low η_c correspond to the colloidal vapor and those at high η_c to the colloidal liquid phase. The region in between is the phase-separated regime. The distributions in Fig. 1 are for the bulk case and were obtained at coexistence, which means that the fugacity z_c was tuned such that the area under both peaks is equal. The height of the barrier marked ΔF in Fig. 1 corresponds to the free energy barrier separating the coexisting phases⁵. This barrier is related to the interfacial tension γ via $\gamma = \Delta F/(2A)$ (with $A = L_x \times L_y$ the area of the interface) provided that the size of the system is large enough. The factor $1/2$ in the latter equation for γ stems from the use of periodic boundary conditions that yield the formation of two interfaces in the system (see snapshots in Fig. 1). It is crucial to use an elongated box for an accurate determination of γ since this enforces the flat region seen in the distribution $P(\eta_c)$ which indicates that the two interfaces in the phase-separated regime are well-separated from each other and thus interactions between the interfaces are suppressed. A detailed analysis of the interfacial tension and other interfacial properties such as capillary waves can be found in recent publications^{3,6-8}.

Fig. 2 shows a snapshot of a confined AO mixture for the film thickness $D = 10$ in the phase-separated regime. As one can infer from the figure, the wall effectively attracts the colloids and thus colloid-rich layers are formed at the walls. We have studied how the presence of walls affects the critical behavior of the AO model by determining the phase

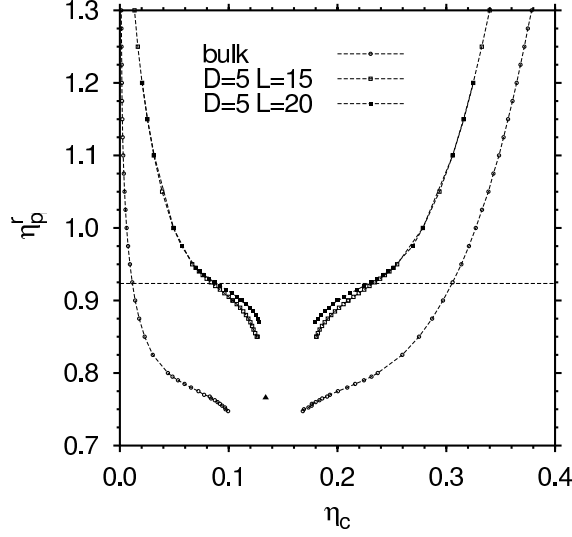


Figure 3. Phase diagram of the AO model with $q = 0.8$ in bulk (open circles) and confinement (open and closed squares for film thickness $D = 5$ for different lateral dimensions L). The black triangle marks the bulk critical point. The dashed horizontal line marks the critical polymer packing fraction of the confined systems in the limit $L \rightarrow \infty$ which is estimated from the cumulant intersection method (see text). From Ref.⁹.

diagrams (binodals) from the probability distributions $P(\eta_c)$ as obtained from the grand canonical MC simulations. To this end, the packing fractions for the colloid vapor and colloid liquid phase, denoted respectively by η_c^v and η_c^l , have been calculated from the probability distributions at coexistence via

$$\eta_c^v = 2 \int_0^{<\eta_c>} P(\eta_c) d\eta_c \quad (1)$$

$$\eta_c^l = 2 \int_{<\eta_c>}^{\infty} P(\eta_c) d\eta_c \quad (2)$$

where $<\eta_c>$ is the first moment of $P(\eta_c)$, $<\eta_c> = \int_0^{\infty} \eta_c P(\eta_c) d\eta_c$.

Fig. 3 shows the binodals for the bulk and for a thin film of thickness $D = 5$ for two different values of L . Since η_p^r plays the role of inverse temperature, the phase diagram appears inverted compared to temperature-density phase diagrams of simple fluids. As the figure demonstrates, confinement shifts the critical point towards higher η_p^r and slightly higher values of η_c . In the vicinity of the critical point pronounced finite size effects are present which can be inferred from a comparison of the curves for $L = 15$ and $L = 20$ in the case of the confined geometry. The critical points that are indicated in the figure were estimated from a finite size scaling analysis using the cumulant intersection method². From the latter method, we have also inferred that properties near the critical point seen in the simulation of the confined AO model can neither be attributed to the 2D nor to the 3D Ising model universality class. This can be intuitively understood in terms of the correlation length ξ that diverges near the critical point: when ξ exceeds the film thickness D , the system becomes effectively two-dimensional, such that a crossover from 2D to 3D

Ising critical behavior is expected. A detailed discussion of this issue can be found in a forthcoming publication⁹.

In summary, we have performed extensive MC simulations to investigate the phase behavior of an AO model in the bulk and in confined geometry. We have demonstrated that the simulation allows an accurate description of interfacial properties and critical phenomena.

3 Interfacial Properties of Colloidal Liquid Crystals

Suspensions of anisotropic particles form liquid crystals at sufficiently high pressure or low temperature. In particular, suspensions of rod-like as well as plate-like particles undergo a phase transition from a phase in which the particle orientations are disordered (“isotropic” phase) to a phase in which there is a direction of preferred alignment (“nematic” phase). In many materials the direction of preferred alignment of the particles can be easily manipulated with electric or magnetic fields, which means that the optical properties of these materials can be tuned. This has made liquid crystals the basis for a large range of technological devices¹⁰.

Liquid crystals also pose fundamental questions about the role which particle anisotropy plays in phase transitions and interfacial properties. In the 1940s Onsager showed that the transition between the isotropic phase (I) and the nematic phase (N) is of entropic nature and that it can be explained by a simple geometrical argument¹⁵. However, the calculation of interfacial properties in the Onsager model proved to be far more difficult than the prediction of the phase transition.

Also, there is a crucial difference between the nematic ordering of rod-like and of plate-like particles: The former may be quantitatively understood at the level of second virial theory (at least for infinite aspect ratios) whereas this is not the case for the latter. Local order differs strongly between platelets and rods. One feature that is affected by this is the isotropic nematic interface (“IN-interface”). We have used the super computing resources in Jülich to investigate the interfacial tension γ_{IN} in suspensions of rods and of platelets. (For an introduction to interfacial tensions in colloidal systems see reference¹⁴.)

As a model for rods we used spherocylinders of length l and diameter d ; as a model for platelets we used cut spheres of thickness l and diameter d . We studied IN-coexistence by means of grand canonical MC simulations, where the volume V , the temperature T , and the chemical potential μ are fixed, while the number of particles in the simulation box fluctuates.

Fig. 4 shows a configuration snapshot taken during a simulation of a suspension of soft spherocylinders. Different orientations are labeled by colour. On the left the system is isotropic, on the right it is nematic. Because of the periodic boundary conditions, there are two interfaces. The interfaces are marked by dashed lines.

Fig. 5 shows the probability distribution $P(\rho)$ of the density of particles in the system. (The quantity plotted on the x -axis, ρ^* is the number density N/V divided by the density at closest packing).

The interfacial tension γ_{IN} turns out to be very small. For rods we find^{11,12} $\gamma_{\text{IN}}^{\text{rods}} = (0.09 \pm 0.01) k_{\text{B}}T/ld$. For platelets the biphasic gap becomes so narrow, that we could only determine¹³ an upper bound for the interfacial tension $\gamma_{\text{IN}}^{\text{platelets}} < (0.013 \pm 0.004) k_{\text{B}}T/d^2$. These numbers are several orders of magnitude smaller than interfacial

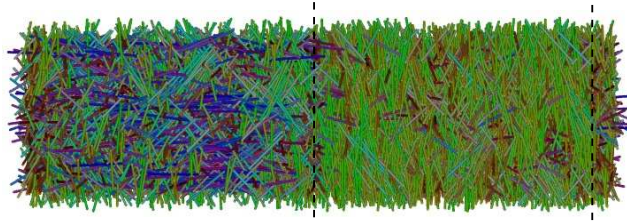


Figure 4. Configuration snapshot of spherocylinders with $l/d=15$. Orientations are labeled by colour. On the left the system is isotropic, on the right it is nematic. The interfaces are marked by dashed lines. (There are two interfaces because of the periodic boundary conditions.)

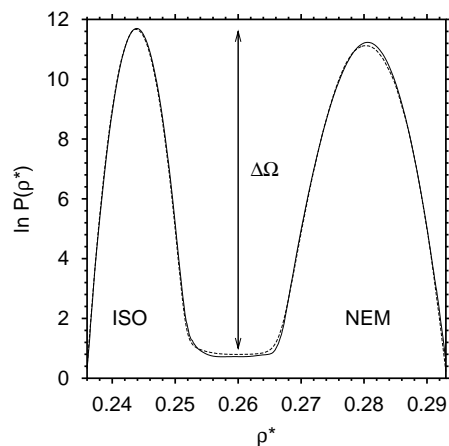


Figure 5. Density distribution at coexistence for soft spherocylinders, $l/d=15$. The tension of the isotropic nematic interface can be determined from the height of the peaks $\Delta\Omega$.

tensions in typical atomistic or molecular systems. This is due to the fact that the IN-interface is of purely entropic origin. Such small interfacial tensions are very difficult to compute in simulations, and we had to develop new sampling techniques to be able to reach these values. Details can be found in¹¹.

In particular, the extremely low value of $\gamma_{IN}^{\text{plates}}$ was surprising. Therefore our collaborators in Utrecht performed an experiment to check the simulation results. In experiments, one standard and popular way to measure an interfacial tension is the “capillary rise method”, where the interfacial tension is determined from the rise of the meniscus between two phases at a hard wall. In general however, this method can not be applied to liquid crystals. The walls and the interface orient the liquid crystal (“interfacial anchoring”), causing deformations of the director field. Platelets anchor homeotropically (i.e. they lie flat) on hard walls and on the IN-interface. The capillary rise is thus determined by a compromise between interfacial anchoring and Frank elasticity.

Before we could interpret our experimental results on the capillary rise, we therefore needed to analyze the elastic contributions. A colloidal suspension of sterically stabilized

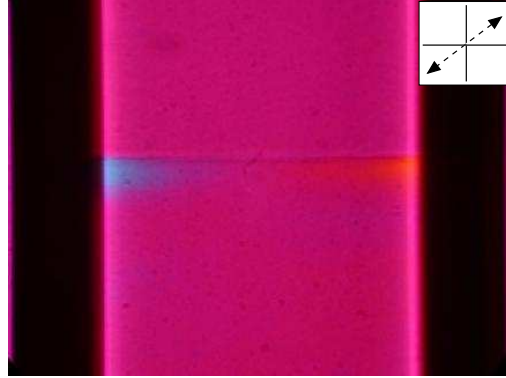


Figure 6. Polarised light micrographs of the IN interface taken between crossed polarisers. Polariser orientation is indicated by the cross. A retardation plate was used to show the orientation of the director field; its slow axis is indicated by the dashed arrow.

gibbsite $[\text{Al}(\text{OH})_3]$ platelets in toluene was synthesized according to van der Kooij and Lekkerkerker¹⁶. To investigate the IN-interface, we prepared a sample of the suspension in the IN-biphasic gap in a $500\ \mu\text{m} \times 500\ \mu\text{m}$ glass capillary¹³. Phase separation occurred over a time scale of a few days; annealing of the domains in the nematic phase took several weeks.

A polarised light microscope was then used to study the IN-interface near the wall and the orientation of the director field in the capillary “foot”, i.e. in the region of risen nematic phase at the wall. Fig. 6 shows a micrograph of the interface taken between crossed polarizers with a retardation plate of $\Delta n D = 530\ \text{nm}$, where Δn is the birefringence and D is the thickness of the sample. A retardation plate permits to obtain the direction of the so-called fast and slow axes in a birefringent sample. Depending on the mutual orientation of slow and fast axes in the retardation plate and in the sample, the retardation due to the plate is either added to or subtracted from the samples’ birefringence. In regions where the slow axis of the sample is parallel to the slow axis of the retardator “addition” occurs and the pink colour shifts to higher orders, i.e. blue. Wherever they are perpendicular, subtraction occurs and the colour becomes orange. In a separate experiment, we found that the slow axis of a well-oriented suspension of our colloidal gibbsite platelets is parallel to the nematic director. In Fig. 6 the slow axis of the retardation plate is indicated by the arrows. The “corners” of the nematic phase are shifted in colour as compared to the bulk, which is pink. Hence we can conclude that the defect of the director field, which would be expected to lie at the contact line, has a large uniform core. Therefore the capillary “foot” is not affected by a bend director field and we can extract γ_{IN} without knowledge of the elastic constants of the sample. (For details of the analysis see¹³.) From the height of the capillary rise we conclude $\gamma_{\text{IN}} < (0.04 \pm 0.02) k_B T / d^2$.

In summary, we have performed computer simulations of the isotropic-nematic interface in colloidal liquid crystals. We have found that the interfacial tension in suspensions of rod-like particles is one order of magnitude larger than in plate-like particles. Our results could be compared to experiments on the capillary rise of the IN-interface without the need to know the elastic constants of the system.

4 Acknowledgments

T.S. and J.H. were supported by MWFZ Forschungsfonds and the Emmy Noether Programm of the Deutsche Forschungsgemeinschaft (DFG). Furthermore, we acknowledge support from SFB TR6, projects A5 and D5. We thank Ronald Blaak for helpful comments. Allocation of computer time on the JUMP at the Forschungszentrum Jülich is gratefully acknowledged. A Part of this work was financially supported by the “Nederlandse Organisatie voor Wetenschappelijk Onderzoek” (NWO).

References

1. S. Asakura and F. Oosawa, Surface Tension of High-Polymer Solutions, *J. Chem. Phys.* **22**, 1255 (1954).
2. D. P. Landau and K. Binder, *A Guide to Monte Carlo Simulations in Statistical Physics* (Cambridge University Press, Cambridge, 2000).
3. R. L. C. Vink and J. Horbach, Grand canonical Monte Carlo simulation of a model colloid-polymer mixture: Coexistence line, critical behavior, and interfacial tension, *J. Chem. Phys.* **121**, 3253 (2004).
4. P. Virnau and M. Müller, Calculation of free energy through successive umbrella sampling, *J. Chem. Phys.* **120**, 10925 (2004).
5. K. Binder, Monte Carlo calculation of the surface tension for two- and three-dimensional lattice-gas models, *Phys. Rev. A* **25**, 1699 (1982).
6. R. L. C. Vink and J. Horbach, Critical behaviour and interfacial fluctuations in a phase-separating model colloid-polymer mixture: grand canonical Monte Carlo simulations, *J. Phys.: Condens. Matter* **16**, S3807 (2004).
7. R. L. C. Vink, J. Horbach, and K. Binder, Critical phenomena in colloid-polymer mixtures: Interfacial tension, order parameter, susceptibility, and coexistence diameter, *Phys. Rev. E* **71**, 011401 (2005).
8. R. L. C. Vink, J. Horbach, and K. Binder, Capillary waves in a colloid-polymer interface, *J. Chem. Phys.* **122**, 134905 (2005).
9. R. L. C. Vink, J. Horbach, and K. Binder, Critical behavior of a colloid-polymer mixture confined between walls, in preparation.
10. P. G. de Gennes and J. Prost, *The Physics of Liquid Crystals* (Clarendon Press, Oxford, 1993).
11. R. L. C. Vink, S. Wolfsheimer, and T. Schilling, Isotropic-nematic interfacial tension of hard and soft rods: application of advanced grand canonical biased sampling techniques, in press (2005).
12. R. L. C. Vink and T. Schilling, Interfacial tension of the isotropic-nematic interface in suspensions of soft spherocylinders, *Phys. Rev. E* **71**, 051716 (2005).
13. T. Schilling, P. van der Schoot, D. van der Beek, R. L. C. Vink, R. van Roij, M. Dijkstra, and H. Lekkerkerker, Ultra-low interfacial tension in suspensions of colloidal platelets, in preparation (2005).
14. P. van der Schoot, Remarks on the interfacial tension in colloidal systems, *J. Phys. Chem. B* **103**, 8804 (1999).
15. L. Onsager, *Ann. N. Y. Acad. Sci.* **51**, 627 (1949).
16. F. M. van der Kooij and H. N. W. Lekkerkerker, *J. Phys. Chem. B* **102**, 7829 (1998).